INTERIM

7N-89-CR

80287

STUDIES OF CLUSTERS OF GALAXIES

NASA GRANT NAG8-287

Annual Reports for
13 January 1994 through 12 January 1995
13 January 1995 through 12 January 1996
and
Final Report
For the Period 12 March 1993 through 11 March 1996

Principal Investigator
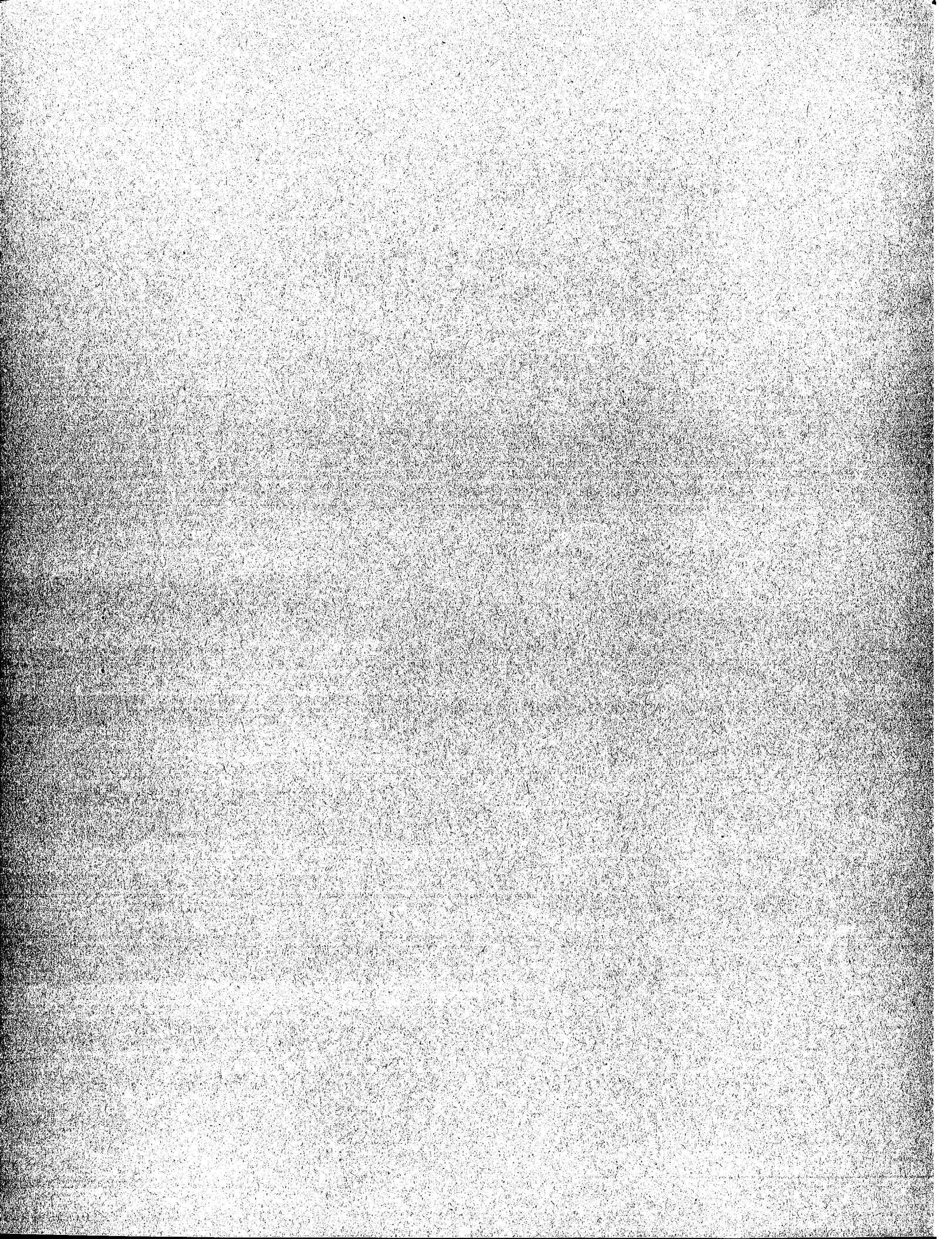Dr. John P. Hughes

August 1996

Prepared for:

National Aeronautics and Space Administration
George C. Marshall Space Flight Center
Marshall Space Flight Center, AL 35812

Smithsonian Institution
Astrophysical Observatory
Cambridge, Massachusetts 02138

The Smithsonian Astrophysical Observatory
is a member of the
Harvard-Smithsonian Center for Astrophysics

The NASA Technical Officer for this grant is Jeannette Vargas, George C. Marshall Space
Flight Center, Code EM25, Marshall Space Flight Center, AL 35812.

Final Report – Grant NAG8-287
August 15, 1996
John P. Hughes

NASA Grant No. NAG8-287 supported the analysis and interpretation of *Ginga* Large Area Counter (LAC) data on the supernova remnant W44 and the Coma cluster of galaxies. Results of this work are described below.

W44

The research on W44 has resulted in a draft publication that is ready to be submitted to *The Astrophysical Journal* titled "Interpretation of the Center-Filled Emission from the Supernova Remnant W44" by Ilana Harrus, John P. Hughes, K. P. Singh, K. Koyama, and I. Asaoka. Please refer to the attached copy of this paper for full details.

Coma Cluster of Galaxies

The *Ginga* LAC accumulated data in scanning mode on this source resulting in a measurement of the temperature profile of the cluster. We used these data in conjunction with other X-ray spectral data from *Tenma* (Hughes *et al.* 1988, *ApJ*, **327**, 615), *EXOSAT* (Hughes, Gorenstein, & Fabricant 1988, *ApJ*, **329**, 82), *Ginga* (Hughes *et al.* 1993, *ApJ*, **404**, 611), and Spacelab-2 (Watt *et al.* 1992, *MNRAS*, **258**, 738) to constrain the binding mass profile of the cluster. The radial profile of Coma from the *ROSAT* All-Sky Survey (Briel, Henry, & Böhringer 1992, *A&A*, **259**, L31) was used too, since the maximum observed extent of the X-ray emission is an important constraint on the mass models. The technique used was one I had developed previously (Hughes 1989, *ApJ*, **337**, 21) that employed parameterized models for the unknown dark matter distribution and the equation of hydrostatic equilibrium to calculate temperature profiles for comparison with the spectral data. In this project, I assumed mass profiles of the form $\rho_D = \rho_{D0}[1 + (R/R_D)^2]^{-p}$ and derived limits on the values of the central binding mass density ρ_{D0}, the core radius of the dark matter distribution R_D, and the index of the profile p. The distributions of luminous matter were included as separate components with their measured profiles. The gas followed the law $5.5 \times 10^{-27} \, \mathrm{gm\,cm^{-3}} \, [1 + (R/10\overset{\prime}{.}5)^2]^{-1.125}$ (Briel *et al.* 1992) while the mass in galaxies was assumed to follow the profile $1.2 \times 10^{-27} \, \mathrm{gm\,cm^{-3}} \, [1 + (R/9\overset{\prime}{.}6)^2]^{-1.5}$. The latter was based on the projected profile from Millington & Peach (1986, *MNRAS*, **221**, 15) and a mass-to-light ratio of 8 $M_\odot/L_\odot$ (Pickles 1985, *ApJ*, **296**, 340).

We explored values of p (the index of the dark matter profile) from 1 to 8 and found that the best-fit was obtained for $p = 8$. We were able to constrain $p > 1.126$ at 99% confidence, a result that shows for the first time with high confidence that the dark matter in the Coma cluster is more centrally concentrated than the gas, which itself is the dominant luminous matter component. A scenario with the dark matter distributed like the galaxies is not a highly favored model and can be rejected at the 90% confidence level.

Within an Abell radius (3 Mpc) we find the dark matter mass to vary between (0.5 −

1.2) $\times 10^{15}\, M_\odot$ (at the 90% confidence level). Within the same radius the luminous matter (gas plus galaxies) has a mass of $3.5 \times 10^{14}\, M_\odot$.

This work was completed recently and is now being prepared for publication in *The Astrophysical Journal.*

Interpretation of the Center-Filled Emission from the Supernova Remnant W44

Ilana Harrus[1,2], John P. Hughes[2,3], K. P. Singh[4], K. Koyama[5], and I. Asaoka[6]

ABSTRACT

We report the results of spectral and morphological studies of X-ray data from the supernova remnant (SNR) W44. Spectral analysis of archival data from the *Einstein Observatory*, *ROSAT*, and *Ginga*, covering a total energy range from 0.3 to 8 keV, indicates that the SNR can be described well by a nonequilibrium ionization (NEI) model with temperature $\sim$0.9 keV and ionization timescale $\sim$6500 cm^{-3} years. All elemental abundances are found to be within about a factor of two of their cosmic values, with iron possibly appearing to show significant depletion. No clear evidence for emission from supernova ejecta can be inferred from the observed metal abundances. The column density toward the SNR is high – around 10^{22} atoms cm^{-2} – as expected given the location of the remnant in the Galactic plane.

In addition to the spectral analysis, we have investigated two different evolutionary scenarios to explain the centrally-brightened X-ray morphology of the remnant: (1) a model involving the slow thermal evaporation of clouds engulfed by the supernova blast wave as it propagates though a clumpy interstellar medium (ISM) (White & Long 1991, hereafter WL), and (2) a hydrodynamical simulation of a blast wave propagating through a homogeneous ISM, including the effects of radiative cooling. Both models can have their respective parameters tuned to reproduce approximately the morphology of the SNR. The mean temperature of the hot plasma in W44 as determined by our

[1]Harvard-Smithsonian Center for Astrophysics, 60 Garden Street, Cambridge MA 02138

[2]Department of Physics, Columbia University, 538 W 120th Street, New York, NY 10027

[3]Department of Physics and Astronomy, Rutgers University, P.O. Box 849, Piscataway, NJ 08855-0849

[4]Tata Institute of Fundamental Research, Homi Bhabha Road, Bombay, 400 005 India

[5]Department of Physics, Kyoto University, Kitashirakawa, Oiwake-cho, Sakyo-ku, Kyoto 606, Japan

[6]Max-Planck-Institute für Extraterrestrische Physik, W-8046 Garching bei München, Germany

NEI X-ray analysis provides the essential key to discriminate between these scenarios. Based on the size (using the well established distance of 3 kpc) and temperature of W44, the dynamical evolution predicted by the WL model gives an age for the SNR of merely 6500 yrs. We argue that, because this age is inconsistent with the characteristic age ($P/2\dot{P} \sim 20000$ yr) of PSR 1853+01, the radio pulsar believed to be associated with W44 (Wolszczan, Cordes, & Dewey 1991), this model does not provide the explanation for the center-filled morphology. We favor the radiative-phase shock model since it can reproduce both the morphology and age of W44 assuming reasonable values for the initial explosion energy in the range $(0.5 - 0.7) \times 10^{51}$ ergs and the ambient ISM density of between 2.0 and 3.3 cm^{-3}.

Subject headings: ISM: abundances – ISM: individual (W44) – nuclear reactions, nucleosynthesis, abundances – shock waves – supernova remnants – X-rays: ISM

1.   Introduction

The study of supernova remnants (SNRs) provides a unique tool with which to deepen our understanding of the interstellar medium (ISM) and the processes which shape its structure, energetics and composition. At the time of their death, stars induce a formidable release of energy into the ISM and a strong shock wave begins to propagate. At early stages of the evolution, the observed emission contains contributions from both the supernova (SN) ejecta and the ISM. One of the major challenges for X-ray spectroscopy of young SNRs is the differentiation and characterization of these two contributions. Knowledge of the composition of SN ejecta is of considerable importance for the constraints it can provide, though the study of nucleosynthesis, on the nature and evolution of the progenitor star. At later stages SNRs and their evolution are dominated by the interstellar medium. In this article we explore the nature of W44, a middle-aged supernova remnant which is in the ISM-dominated stage of evolution.

W44 was first discovered as a radio source in a survey by Westerhout (1958), and was observed later by several others (Mills, Slee, & Hill 1958; Edge et al. 1959). It was identified as a possible supernova remnant by Scheuer (1963) because of its shell-like radio structure and its non-thermal radio spectrum. OH and H I absorption measurements (Gross 1968; Gross, Caswell, & Robinson 1971; Radhakrishnan et al. 1972; and Knapp & Kerr 1974) have resulted in a more complete mapping of the heavily obscured surroundings of the SNR and lead to the widely accepted distance of 3 kpc to the remnant. The 20 cm VLA image shows a roughly elliptical limb-brightened radio shell with minor and major semi-axes of 10 pc and 15 pc for this assumed distance (Jones, Smith, & Angellini 1993). Knots and filaments contributing to the emission are also seen; Jones et al. (1993) have interpreted these as arising from the radiative shocks driven into interstellar clouds. The radio emission is non-thermal with a spectral index of -0.3 and it is highly polarized ($> 20\%$, Kundu & Velusamy 1972) .

There are two radio pulsars in the vicinity of W44. One of them, PSR 1854+00 (Mohanty 1983), is old (10^8 yr), which makes an association between it and the remnant unlikely. The discovery of the other pulsar, PSR 1853+01, is more recent (Wolszczan, Cordes, & Dewey 1991). Taylor, Manchester, & Lynn (1993) give a distance to this pulsar of 3.3 ± 0.3 kpc while the dispersion-measure distance (Taylor & Cordes 1993) is 2.8 ± 0.1 kpc, both of which are in excellent agreement with the distance estimate to W44 mentioned above. There is a radio synchrotron nebula associated with PSR 1853+01 (Jones et al. 1993, Frail et al. 1996); in addition an X-ray counterpart to the nebula has been recently announced (Harrus, Hughes, & Helfand 1996). This is a young pulsar: it exhibits large timing noise and the ratio of the period to period derivative, the characteristic spin-down

age of the pulsar, is $\sim$20000 years. Given that one can reliably associate the pulsar and the SNR W44, this provides a independent estimate of the remnant's age, which, as we show below, offers an extremely valuable piece of information for discriminating between evolutionary scenarios.

W44 was discovered as an X-ray source by the Astronomical Netherlands Satellite (Gronenschild et al. 1978), and has been a popular target of all subsequent X-ray astronomy satellites. Smith et al. (1985) presented the first detailed X-ray imaging observations based on data from the imaging proportional counter (IPC) onboard the *Einstein Observatory*. In the soft X-ray band W44 presents a centrally-peaked morphology, which is more reminiscent of a pulsar-driven synchrotron nebula (like the Crab Nebula) than a shell-type SNR (like the Cygnus Loop). However the X-ray spectrum of W44 (Jones et al. 1993; Rho et al. 1994) is predominantly thermal in origin, based on the presence of strong emission lines from highly ionized atoms of magnesium, silicon, sulfur, and iron clearly observed by the *Einstein* solid state spectrometer (SSS). The presence of PSR 1853+01 and its associated synchrotron nebula notwithstanding, W44 belongs to the class of "center-filled" remnants which show limb-brightened radio shells, centrally-peaked X-ray morphologies, and predominantly thermal X-ray spectra.

In the Sedov (1959) model of supernova remnant evolution, the SN blast wave propagates through an isotropic homogeneous ISM. At the shock-front the swept-up material is heated to temperatures of order 10^7 K and results in a shell-like X-ray morphology with a thermal spectrum. The limb-brightened radio emission comes from compression of the interstellar magnetic field and accompanying acceleration of electrons which also occurs at the SNR shock front. This simple model, although apparently successful for the numerous known shell-like SNRs, fails to account for remnants such as W44, which have a distinct, centrally-peaked X-ray morphology.

Other models have been proposed to explain the observed morphology of W44 and other remnants of this type. In one particular scenario the remnant is in a later phase of evolution when the blast wave has gone radiative (shock velocities of roughly 300 km s^{-1}, Cox 1972). The radio shell traces the position of the shock front, but, since the X-ray emission from the shock front is soft ($kT \sim 10^6$ K) and the line-of-sight ISM column density is significant ($\sim 10^{22}$ atoms cm^{-2}), the outer shell is essentially invisible in the X-ray band (Smith et al. 1985). The X-ray emission comes rather from the hot interior of the remnant, providing a center-filled morphology. This model predicts that W44 should be old and that the X-ray temperature should decrease from the center of the SNR out to the edge. Some support for this scenario comes from the recent discovery of Hα and S ii emitting optical filaments around the periphery of the X-ray emission (Rho et al. 1994) and an expanding shell of H i emission (Koo & Heiles 1995), indicating the presence of cool gas there. In the White & Long (1991) (WL) scenario, the SNR is expanding into a cloudy

ISM (as in the ISM models of McKee & Ostriker 1977) and evaporating clouds produce an increased density of hot gas in the interior, giving the centrally-peaked appearance. Here the temperature is expected to be relatively uniform throughout the interior.

In this article we explore the implications of these two evolutionary scenarios for W44 using constraints obtained from X-ray imaging and spectroscopic observations from the *Einstein Observatory*, *ROSAT*, and *Ginga*. The next section consists of a brief summary of current knowledge on the SNR in the X-ray band, and of the observations used in our analysis. Our models and the analysis techniques which provide the relevant observational constraints are presented in § 3. We apply these constraints to W44 in the context of the two proposed evolutionary scenarios in § 4. A summary of the paper's main points is to be found in § 5.

2. X-ray Observations of W44

2.1. *ROSAT* PSPC

The first set of data to be described comes from the position sensitive proportional counter (PSPC) (Pfeffermann et al. 1986) onboard *ROSAT* (Trümper 1983). The PSPC spectral resolution ($\Delta E/E$) was about 45% (FWHM) at 1 keV and the instrument was sensitive over the energy band 0.1–2.4 keV. W44 was observed by the PSPC in April 1991. Note that these data were also analyzed by Rho et al. (1994).

We extracted the PSPC data from the *ROSAT* archive and carried out the following reduction procedures. First we applied a time filter to reject data during orbital periods contaminated by solar X-rays scattered into the telescope field of view by the upper atmosphere. These periods manifest themselves as sudden increases in the total count rate at the beginning or end of the good time intervals supplied as part of the *ROSAT* standard processing. After rejecting these time periods, the deadtime-corrected exposure time was 6726 s. In order to minimize contamination due to particle-induced background, it has been recommended that data be rejected during time intervals when the master veto rate is greater than 170 s^{-1} (Snowden et al. 1994). Since only 3% of our remaining data had an associated master veto rate above this threshold, we decided not to apply an additional time filter to reject those events. We also restricted our analysis to the central 40' region of the detector.

The W44 source spectrum was extracted from within the region defined by the surface brightness contour corresponding to 10% of the peak brightness. The background region lay outside this, but still came from within the central region of the PSPC (within the window support ring). The background spectrum was corrected for the energy-dependent

difference in detector response (mainly due to off-axis vignetting) between the source and background regions and was normalized by the ratio of solid angle between the regions. After background subtraction, the total PSPC count rate of W44 is 4.22 ± 0.02 s^{-1}. The PSPC spectrum of the entire remnant is shown in Figure 1. A fit to these data using a solar abundance, collisional equilibrium ionization thermal plasma model (Raymond & Smith 1977; 1992 July 27 version, hereafter RS) provided an unacceptable fit with a χ^2 of 39 (for 19 degrees of freedom). In this case, the best-fit temperature, kT, was ~ 1 keV and the column density, N_H, was 7.9×10^{21} cm^{-2}.

2.2. *Einstein* SSS

The *Einstein* solid state spectrometer (SSS) has been described in detail by Joyce et al. (1978) and Giacconi et al. (1979); here we provide only a brief discussion of its main characteristics. The SSS was sensitive to X-rays between 0.4–4.0 keV with a nominal spectral resolution (FWHM) varying from 30% at low energies to 4% at high energies. During orbital operations, an unexpected problem of ice formation on the detector window occurred, which caused a time dependence in the low energy efficiency of the SSS. An empirical model for this effect has been developed based on the analysis of a number of observations of the Crab Nebula taken throughout the course of the *Einstein* mission (Christian et al. 1992); in this work we employ the nominal ice absorption model appropriate to the dates of observation of W44.

The total SSS exposure time on W44 was 22608 sec. The data were acquired in four separate pointings toward two different regions of the remnant. (Note that the field of view of the SSS was about 6′ in diameter and thus a single pointing did not cover the entire SNR.) The four datasets were compared and, since they were consistent with each other within the statistical errors, they were summed to form a single spectrum. The separate response functions were averaged (weighting by each pointing's exposure time). A total of 8072 source photons were detected. In order to account for systematic uncertainties in the ice absorption model, as well as other uncertainties in the SSS calibration, we have added a systematic error equal to 2% of the source intensity in each spectral bin. The minimum energy we consider for this data set is 0.8 keV. The SSS spectrum in Figure 1 shows obvious emission lines from Kα transitions of highly ionized atoms of magnesium, silicon, and sulfur, which clearly points to a thermal origin for the X-ray emission. Nevertheless this spectrum cannot be fit well by a simple solar abundance RS thermal plasma emission model. The reduced χ^2 of 4.5 obtained in this case (for $kT \sim 0.9$ keV and $N_H = 7.4 \times 10^{21}$ cm^{-2}) indicates that a more detailed analysis, including such effects as nonequilibrium ionization, is necessary.

2.3. *Ginga* LAC

The major experiment on *Ginga* (Makino et al., 1987) was the Large Area Counter (LAC) (Turner et al. 1989), an array of eight sealed proportional counters with a total geometric collecting area of 4000 cm^2, mechanically collimated to a field of view of 1° by 2° (FWHM). The efficiency of the LAC for collecting X-rays was high (greater than 10%) over the 1.5–30 keV band. The lower energy limit was defined by the thickness of the Be window material ($\sim$62 μm), while the high energy limit arose from the finite active depth of the proportional counter gas volume. These detectors had an energy resolution of 18% (FWHM) at about 6 keV. With its very low internal background rate and large effective area, the LAC was a very sensitive instrument for carrying out X-ray spectral studies.

No direct pointing of W44 was made by *Ginga*. Rather we have extracted data on the source from a scan of the Galactic plane carried out on 12 September 1988. Scan data were taken in MPC2 mode, which combined the data from the top and middle layers of the LAC and summed the data from four detectors into one before telemetering to the ground. The two spectra so obtained were summed during data reduction. Background was determined from source-free regions of the scan on both sides of W44. The effective exposure time was low (1984 s), however the source is bright ($\sim$15 counts s^{-1}), and the X-ray spectrum is well-defined from 1.5 keV to 10 keV. The spectrum is soft, consistent with a RS thermal model with $kT \sim 0.75$ keV and an interstellar column density of $\sim$10^{22} cm^{-2}. There is no evidence for any harder emission component in the *Ginga* data. We set an upper limit (3 σ) of 3.6×10^{-12} ergs cm^{-2} s^{-1} to the 2–10 keV flux of a Crab-like power-law component ($dN/dE \sim E^{-2.1}$) contributing to the *Ginga* spectrum of W44.

2.4. Other Observations

During the initial phases of this study, we explored the possibility of using X-ray observations of W44 from other sources of archival data, namely from the *Einstein Observatory* and *EXOSAT*. After careful evaluation it became clear that these data would not be useful in our study. We review our arguments for arriving at this conclusion below.

The *Einstein* imaging proportional counter (IPC) is similar to the *ROSAT* PSPC in many respects. The major advantage of the IPC over the PSPC is its higher energy cutoff (4.5 keV vs. 2.4 keV). This advantage, however, is largely offset by the IPC's poorer energy resolution and image quality, and the large uncertainty in its calibration which limits its usefulness for detailed spectral analysis. In our preliminary spectral fits, it was found that the IPC global spectrum was consistent with that from the PSPC and SSS, although the best-fit χ^2 for the IPC data was formally unacceptable. Although consistent with the other

data, the IPC spectrum does not provide additional constraint on the model and thus we reject it as being redundant.

Data from the medium energy (ME) proportional counters on *EXOSAT* are available through the High Energy Astrophysics Science Archive maintained by the Goddard Space Flight Center (GSFC). The data in this archive have undergone a standard reduction procedure to produce background-subtracted spectral files for analysis. The processing flag for the ME spectrum of W44 is listed as quality 2, which indicates a major problem with the reliability of the data. Indeed the ME spectrum of W44 shows a hard component above about 5 keV and a reasonably strong Kα iron line, both of which are entirely absent in the *Ginga* LAC spectrum.

The problem with the standard background subtraction for the W44 data was identified by Jones et al. (1993), who examined the raw ME data and found that a significant fraction of it was contaminated by irregular count rate flares presumably induced by penetrating charged particles. After rejecting the data from the most seriously affected detectors, Jones et al. (1993) obtained good fits to the ME data of a single temperature RS thermal model with $kT \sim 0.9$ keV and $N_\mathrm{H} \sim 10^{22}$ cm^{-2}. These results are consistent with those derived using the *Ginga* data. Because we had no access to the raw *EXOSAT* data and since the *Ginga* LAC covers the same energy band and is therefore fully complementary, we decided to exclude the ME data altogether.

In their complex analysis of W44 Rho et al. (1994) use the contaminated ME data obtained directly from the GSFC archive. This explains why these authors require a high temperature component in their model fits. It also likely invalidates the conclusions they arrive at concerning their best-fitting NEI spectral model (i.e., shock temperature, ionization timescale, and assumptions about electron-ion temperature equilibration timescales).

3. Nonequilibrium Ionization Modeling and Analysis

Accurate plasma diagnostics are the key to our understanding of the physical phenomena which occur during supernova remnant evolution. At the simplest level, measurements of plasma temperature and elemental abundances allow one to derive quantitative values for the plasma density in the SNR from the intensity and brightness distribution shown by broadband X-ray images. Furthermore, as we show below, the remnant's radius, temperature, and density are essential quantities for understanding its dynamical state. The relative abundance ratios of the X-ray emitting plasma, as determined by spectroscopy, can indicate the presence of reverse-shocked ejecta, again providing clues to the evolutionary state of the remnant.

Interpretation of SNR X-ray spectra is complicated by the nonequilibrium processes

that occur in shock heated plasmas and which necessitate detailed time-dependent models of the spectral emissivity. One important influence on the thermodynamic state of the plasma is the fact that the ions are not instantaneously ionized to their equilibrium configuration at the temperature of the shock front. Rather the timescale for attaining full equilibrium ionization is comparable to the remnant dynamical timescale. Numerous authors have incorporated this nonequilibrium ionization (NEI) effect into models of SNR spectral emissivity. Here we use the matrix inversion method developed by Hughes & Helfand (1985) to solve for the time dependent ionization fractions, which has been coupled to the RS plasma emission code (see Hughes & Singh 1994 for more details). The column density of neutral hydrogen along the line-of-sight, N_H, is included as a fit parameter using the cross sections and ISM abundances from Morrison & McCammon (1983).

3.1. Single-temperature, single-timescale NEI model

The simplest NEI model assumes that the X-ray emitting plasma was impulsively heated to temperature kT some time t ago. The temperature, which refers to that of the electrons, is assumed to remain constant. The ionization state actually depends on the product of electron density and age, i.e., the ionization timescale, $\tau_i \equiv n_e t$. We refer to this as the single-temperature, single-timescale NEI model and here we apply it to the spectrum from the entire remnant.

Model fits can, in principle, constrain individual elemental abundances. In practice, some of the individual contributions are not easily separated, especially for those species that are primarily continuum contributors. Therefore, for the elements He, C, N, and O we have fixed the abundance to the solar values relative to hydrogen. The abundances of the other elemental species were allowed to vary freely. For solar abundances we assume the values from RS.

Figure 1 shows the data and best-fit NEI model obtained when the three data sets are fitted jointly. The minimum χ^2 is 137.4 for 92 degrees of freedom. The χ^2 associated with the PSPC data is 25.4 (22 data bins), with the SSS data is 87.0 (72 data bins), and with the LAC data is 25 (11 data bins). The overall normalization of the spectral data provides a value for the emission measure of the hot plasma in W44: $n_H^2 V/(4\pi D^2) = (1.76 \pm 0.37) \times 10^{13}$ cm^{-5}. The best-fit values for the global spectral parameters are temperature, $kT = 0.88 \pm 0.14$ keV; ionization timescale, $\tau_i = (2.0^{+4.3}_{-0.7}) \times 10^{11}$ cm^{-3} s; and column density, $N_H = (1.0^{+0.6}_{-0.2}) \times 10^{22}$ atoms cm^{-2}. The quoted error bars are at the 90% confidence level for three interesting parameters ($\Delta\chi^2 = 6.25$). Figure 2 shows graphically how χ^2 varies with each of these global parameters (also allowing all other parameters to vary freely). Table 1 provides a numerical summary of the abundance results. The first column gives the best-fit elemental abundances, relative to their cosmic values.

The second column shows the errors in abundance determined with the temperature, ionization timescale, and column density fixed at their best-fit values. The remaining columns gives the errors in abundance arising from the variation in the global spectral parameters as shown in Figure 2.

The ionization timescale we derive for W44 is representative of that from a middle-aged remnant (like N132D in the LMC, see Hwang et al. 1993) and is indicative of a plasma that is underionized for its temperature. From the *ROSAT* image, we estimate the mean electron density in the hot plasma (see below) to be $\langle n_e^2 \rangle^{1/2} \simeq 0.4$ cm^{-3}. Combined with the ionization timescale, this suggests an "age" of $\sim$15000 yrs, in good agreement with other estimates of the age of W44 and PSR 1853+01 (see below).

3.2. Radial Temperature Gradient

Some evolutionary scenarios for SNRs (e.g., Sedov) predict significant radial variations in the plasma temperature, while others (e.g., WL) do not. We have used the *ROSAT* PSPC data to constrain the allowed range of temperature variation in W44 in the following approximate manner. Two PSPC spectra were extracted: one from within a radius of 6.'7 and the other from without. Note that the boundary between the regions was chosen so that each spectrum had roughly the same statistical level; the results are not sensitive to the exact position of the boundary. Each PSPC spectrum was fitted to an independent NEI model, and the sum of these NEI models was required to fit the LAC and SSS data. These latter two datasets were assumed to be representative of the entire remnant (which is strictly correct for the LAC data, but only approximately true for the SSS). The NEI models were constrained to have the same abundances, column density, and ionization timescale with values fixed to the best-fit ones determined above, while the temperatures and intensity normalizations of the models describing the two regions were allowed to vary independently. We obtain a better fit if the inner region is somewhat hotter than the outer region. At 90% confidence, the temperature of the inner region is constrained to be between 10% and 20% higher than the temperature of the outer region. This analysis indicates that there is little variation in temperature with position in the remnant, a result that is consistent with previous studies (Rho et al. 1994).

3.3. Multiple NEI Components

In addition to the simple single-temperature, single-timescale NEI model discussed above, we also have investigated the possibility that the X-ray emitting plasma in W44 is in a more complex state. First, we looked for evidence that the ionization state varies

as a function of elemental species. In this study we had two ionization timescales as free parameters: one for a particular individual species (Ne, Mg, Si, S, Ar, and Fe each in turn) and the other for all the remaining elemental species. Fits were carried out with the other relevant spectral parameters (kT, $N_{\rm H}$, and abundances) constrained to be the same for all species and allowed to vary freely. The derived χ^2 values were compared to the single-temperature, single-timescale results to assess the significance of the introduction of the new parameter. None of the elemental species for which we pursued this analysis showed a statistically significant result, suggesting that the various elements contributing to the X-ray emission are uniformly mixed throughout the plasma.

We also carried out fits of a two-component NEI model to the entire spectrum to see whether our data require that the plasma in W44 be multi-phase. The components had the same abundance set and absorbing column density. We assumed that the media were in pressure equilibrium which allowed us to relate the ionization timescales and temperatures as $\tau_{i,2} = \tau_{i,1} kT_1/kT_2$. Note that we also made the implicit assumption that the two components were shocked at the same time. With this condition, only two additional free parameters were introduced: the second temperature and the ratio of emission measures between the two media. We explored values for the temperature of the second component from 0.5 to 5 keV and the ratio of emission measure from 0.1 to 10. Over this range of parameter space, no statistically significant reduction in χ^2 was observed, although equally good fits were obtained in many cases. Our data allow a second component with $kT = 2$ keV only if its emission measure is less than $\sim$3% that of the main component. The allowed emission measure for the addition of a 5 keV component is even more restricted: <0.5% of the main component. Because of the significant interstellar cutoff our limits on gas at temperatures with $kT < 0.5$ keV are rather weak.

3.4.   Volume, Density, Pressure, and Mass Estimates

In the soft X-ray band W44 is roughly elliptical in appearance with a long dimension of 32.'7 and a short one of 19.'7. We estimate the volume of the remnant as an ellipsoid with principal axes in the plane of the sky with sizes as observed. The length of the third axis is some factor, α, times the size of the observed short dimension. This corresponds to a volume, $V = 1.3 \times 10^{59} \alpha D_{3\,\rm kpc}$ cm^{-3}, for the nominal distance to W44 of 3 kpc.

The root-mean-square electron density can be determined simply from the fitted emission measure (§3.1) and the volume. We obtain

$$\langle n_e^2 \rangle^{1/2} = 0.42 \, (\alpha f D_{3\,\rm kpc})^{-1/2} \text{ cm}^{-3}$$

where f is the volume filling factor of the hot plasma and we use a value of 1.09 for the ratio $n_e/n_{\rm H}$. The uncertainty on $\langle n_e^2 \rangle^{1/2}$ from errors in the fitted emission measure alone is ± 0.06 cm^{-3}. The average thermal pressure in the remnant is roughly 1.1×10^{-9} ergs cm^{-3}, assuming that the ion and electron temperatures are equal.

The mass of X-ray emitting hot plasma is given by

$$M = 56\,(\alpha f)^{1/2}\,D_{3\,{\rm kpc}}^{5/2}\;M_\odot.$$

3.5. Abundances

Vancura et al. (1994) argue for the use of depleted abundances when interpreting the X-ray spectra of SNRs, due to the long timescales for grain destruction within the shock heated gas. In their models, the proportion of intact silicate and graphite grains remaining after being engulfed by a blast wave depends strongly on the shocked column N_S, but only weakly on the shock velocity. For W44 we approximate N_S by the product of the RMS density and the mean observed radius, which gives a value $N_S \sim 1.5 \times 10^{19}$ cm^{-2}. The fraction of initially depleted mass remaining in the solid phase for this shocked column is 30–45% (Vancura et al. 1994), implying that the observed abundances of Mg, Si, S, and Fe in W44 should be slightly below solar (abundances of 60–80%). The relatively inert elements Ne and Ar should show no depletion.

Our best fit to the X-ray spectrum of W44 implies elemental abundances that are close to or somewhat below the solar values (except for iron), and in general agreement with the picture sketched above. The strongest apparent depletion is observed for iron, although we are wary of this result due to uncertainties in the atomic physics of iron L-shell emission. It is also true that the iron abundance varies dramatically with changes in the global spectral fit parameters, as clearly shown in Figure 2. For $N_{\rm H}$ values slightly higher than the best fit one (but still within the allowed range), all derived elemental abundances are within a factor of ~ 2 of solar.

On the other hand it is slightly puzzling that the observed abundance pattern shows no clear evidence for the presence of SN ejecta. Models of nucleosynthesis in massive stars (ZAMS masses of 13–25 $M_\odot$) predict the ejection of, for example, 0.047–0.116 $M_\odot$ of Si and 0.026–0.040 $M_\odot$ of S (Thielemann et al. 1996). In total for W44 we observe only about 0.03 $M_\odot$ of Si and 0.01 $M_\odot$ of S and most of this, we have just argued, can be attributed to the swept-up interstellar medium. Perhaps this suggests that the progenitor of W44 is less massive than 13 $M_\odot$, although a lower bound of 8 $M_\odot$ seems necessary in order to produce the neutron star in the associated PSR 1853+01 (Wheeler 1981). The fate of the metals ejected by a SN is also complex: adiabatic cooling during the initial free expansion phase,

subsequent heating by the reverse shock, radiative cooling, the disruption of the ejecta, and so on. As interesting as these issues are, addressing them is certainly beyond the scope of this work and, observationally, will require data of considerably higher spatial and spectral quality than available now.

4. Evolutionary State of W44

The radio image of W44 (Jones et al. 1993, Frail et al. 1996) shows an elliptical-shaped limb-brightened morphology with a size of $34'\!.8 \times 24'\!.4$. In the models we consider below we use the boundaries of the radio emission to delineate the position of the blast wave, employing the mean radius $R_s = 13.1\,\mathrm{pc}\,(\theta_s/15')(D/3\,\mathrm{kpc})$ in our calculations. The X-ray emission from W44 is also elliptical in shape, although centrally peaked, and lies entirely within the radio shell. The elliptical nature of the emission region implies that the models used, which are spherically symmetric, cannot be completely valid. Nevertheless, as a good first approximation, we compare the radially averaged surface brightness profile from the *ROSAT* PSPC with predictions from the models.

4.1. The W44/PSR 1853+01 Association

In the PSR 1853+01 discovery paper (Wolszczan et al. 1991), the arguments for associating the pulsar and the SNR W44 were first laid out: positional coincidence, agreement in inferred distance, the youth of the pulsar as indicated by the observed large timing noise, and agreement between the characteristic spin-down age of the pulsar and the dynamical age of the remnant. More recent research has provided additional strong evidence to support this association. Frail et al. (1996) have imaged the radio synchrotron nebula around PSR 1853+0.1, which they find to show an unusual cometary morphology with the pulsar located near the narrow (southern) end of the nebula. The thermal pressure necessary to confine the radio nebula is roughly 6×10^{-10} ergs cm^{-3} which is within a factor of two of our pressure estimate from the hot gas in W44 (§3.4 above), while it is several orders of magnitude larger than the pressure of the interstellar medium in general. This measurement can leave little doubt that PSR 1853+0.1 lies within the hot X-ray emitting plasma of W44 and that, consequently, the pulsar and SNR were formed in the same supernova explosion.

As we show below, when that SN explosion occurred is critical to our understanding of the evolutionary state of W44. One estimate is provided by the spin-down age of the pulsar. The spin-down of pulsars is believed to follow the relation $\dot{\nu} = -K\nu^n$, where ν is the rotation rate, n is the breaking index and K depends on the properties (such as the

moment of inertia and magnetic field) of the neutron star. A value of $n = 3$ is expected if the pulsar's rotational energy is lost purely through radiation from a dipole magnetic field. Assuming K and n to be constant, one derives the age t of the pulsar

$$t = \frac{P/\dot{P}}{(n-1)} \left[1 - \left(\frac{P_0}{P} \right)^{n-1} \right]$$

in terms of the initial spin period P_0 and the current period P and period derivative $\dot{P}$. The breaking index has been measured for three young pulsars: the Crab (PSR B0531+21), PSR B0540−69 and PSR B1509−58, and all show values less than 3 for n: 2.51 ± 0.01 (Lyne, Pritchard, & Smith 1993), 2.20 ± 0.02 (Boyd et al. 1995), and 2.837 ± 0.001 (Kaspi et al. 1994), respectively. Recently Lyne et al. (1996) measured the breaking index of the Vela pulsar, which is roughly 10 times older than the pulsars mentioned above and in that sense most closely resembles PSR 1853+0.1, and found a surprisingly low value for the index $n = 1.4 \pm 0.2$. Nonetheless Lyne et al. (1996) claim that the age derived using this breaking index and a low initial spin period (20 ms, the estimated initial spin period of the Crab) results in a value that is consistent with other estimates of the age of the Vela SNR.

The radio timing parameters of PSR 1853+0.1 are $P = 0.26743520599(6)$ s and $\dot{P} = (208.482 \pm 0.006) \times 10^{-15}$ s s^{-1} (Wolszczan 1995). Assuming a low initial spin period of 20 ms we estimate an age for PSR 1853+0.1 of 2.65×10^4 yr with $n = 2.5$. If $n = 1.5$, the age estimate is increased significantly to 5.9×10^4 yr. In order for PSR 1853+0.1 to be younger than ∼10,000 yr, then it must have been born as a slow rotator with a spin period $\gtrsim 200$ ms or have undergone an unusual spin-down history. Although not inconceivable, this would make the pulsar in W44 different from the other known pulsars in SNRs discussed above.

4.2. White & Long Model

The WL similarity solution for the evolution of SNRs invokes a multi-phase medium for the interstellar medium consisting of cool dense clouds embedded in a tenuous intercloud medium. The blast wave from a SN explosion propagates rapidly through the intercloud medium, in the process engulfing the clouds. In the model, these clouds are destroyed by gradually evaporating on a timescale set by the saturated conduction heating rate from the post-shock hot gas. Since this timescale can be long, it is possible for cold clouds to survive until they are well behind the blast wave and thus can significantly enhance the X-ray emission from near the center of the remnant.

The timescale for cloud evaporation is one of the two parameters in the WL model in addition to the three parameters which characterize the standard Sedov solution (explosion

energy E_0, ISM density n, and SNR age t). This timescale, which is expressed as a ratio of the evaporation timescale to the SNR age, $\tau_e \equiv t_{\mathrm{evap}}/t$, can depend on various factors, such as the composition of the clumps and the temperature behind the shock front. The other new parameter, C, represents the ratio of the mass in clouds to the mass in intercloud material. For appropriate choice of these two new parameters the model can produce a centrally peaked X-ray emission morphology. Alternatively, other choices of the τ_e and C can reproduce the standard Sedov solution. This model has been applied to the centrally-peaked remnants W28 and 3C400.2 (Long et al. 1991), as well as to CTA1 (Seward, Schmidt & Slane 1995).

We searched the C-τ_e plane of parameter space to determine which values gave a good match to the W44 radial X-ray brightness profile. We integrated the differential equations for the WL similarity solution to obtain the radial run of temperature and density throughout the interior of the remnant. These functions were normalized to their values at the shock front. The temperature at the shock front T_s was related to the emission-measure-weighted temperature $\langle T \rangle$, which we measure, using equation (23) in WL. The density at the shock front n_s was scaled to match the observed emission measure of X-ray emitting gas in W44. For each set of C and τ_e values, appropriate values for T_s and n_s were calculated. With these values and the radial run of temperature and density it was possible to calculate the detailed radial X-ray brightness profile. For each radial bin in the SNR model, a RS plasma model of appropriate temperature was calculated, and the resulting photon spectrum was multiplied by the energy-dependent ISM absorption function assuming our best-fit column density. The absorbed spectrum was convolved with the PSPC efficiency and spectral resolution functions and then projected to the plane of the sky. This was iterated over all radial bins of the model.

Values of C and τ_e in the ratio of approximately 2.5:1 for $5 \lesssim C \lesssim 100$ provided reasonable profiles. In Figure 3 we show the observed PSPC surface brightness profile along with several representative WL models. The dashed curves bracket the range of acceptable solutions: the top one is too centrally peaked, while the bottom one is too limb-brightened. The three curves near the center show examples of good fits.

The dependence of remnant age t on shock radius and temperature T_s in the WL model is identical to that of the Sedov solution:

$$t = 5490 \, \mathrm{yr} \left(\frac{\theta_s}{15'} \right) \left(\frac{D}{3 \, \mathrm{kpc}} \right) \left(\frac{kT_s}{1 \, \mathrm{keV}} \right)^{-1/2},$$

which explicitly includes the functional dependence on distance D. For the allowed range of C and τ_e values, the shock temperature varies between 0.53 keV and 0.95 keV, including observational error on kT. This yields an age for W44 between 5600 yr and 7500 yr, which

is similar to previous estimates of the age of W44 based on application of the WL model (Rho et al. 1994). The square root dependence of t on kT_s means that the temperature would have to be an order of magnitude less than the value we actually measure to increase the remnant's age by a factor of 3. We can think of no systematic effect in our data or analysis that could result in such an enormous change in the mean temperature of W44. Note that the age of the remnant in this scenario also depends on distance. However, in order for W44 to be ~20,000 yr old, the remnant would need to be 2.5 times further away than the accepted distance of 3 kpc. This too is highly unlikely.

Although this model appears to reproduce the intensity and morphology of W44, it predicts an age which is much less than the characteristic age of the associated pulsar. In addition we also find that the estimated initial explosion energies of the acceptable WL models is rather small: $(0.11 - 0.16) \times 10^{51}$ ergs. These two results considerably weaken the plausibility of the WL model as an accurate description of the SNR W44, particularly in comparison to the model we discuss next.

4.3. Radiative Shock Model

To study this alternative evolutionary scenario quantitatively we use a one-dimensional, spherically symmetric, hydrodynamic shock code (Hughes, Helfand, & Kahn 1984). We include radiative cooling parameterized by temperature as in Raymond, Cox, & Smith (1976) for material with solar abundances. Models were generated for a range of values for the initial explosion energy E_0 and ambient ISM Hydrogen number density n, assumed to be homogeneous, isotropic, and free of magnetic fields. For completeness we have considered two extreme cases for the exchange of energy between the shock-heated ions and electrons: (1) rapid equilibration in which the electrons and ions attain the same temperature instantaneously at the shock front and (2) equilibration on a timescale set by Coloumb collisions. We find no difference between these cases for the models that best describe W44 and so only quote results for the Coloumb equilibration models.

The hydrodynamic calculation was initiated using a homologously expanding, uniform density shell of ejecta with a total mass of 10 $M_\odot$ extending over a small spatial extent (from the center of the explosion to a radius of 0.2 pc). At the ages of interest for our modeling of W44, the reverse shock has passed completely through the ejecta, fully thermalizing it. It is well known that a decelerating ejecta shell is Rayleigh-Taylor unstable and observations of young ejecta-dominated SNRs such as Cas A and Tycho show clear evidence that this instability indeed operates in nature. The effect of the instability is to cause significant clumping of the ejecta shell that ultimately results in its fragmentation and disruption. Our simple one-dimensional calculation is unable to model this effect. However, our interest is studying the onset of dense shell formation at the blast wave and not the fate of the

SN ejecta, so this limitation of our calculation is not important. When calculating the projected surface brightness we remove radial bins containing the modeled ejecta, replacing them with an extrapolation of the temperature and density profile from the solution further out, guided by the radial run of temperature and density expected from the Sedov (1959) solution. This effectively removes the ejecta from the calculation. In practice, much of the ejecta should remain within the interior of the remnant and, by increasing the metallicity of the gas there, enhance the central X-ray emission. Whether the centrally peaked brightness of W44 and other SNRs in this class can be explained by enhanced metallicity in the remnant interior is beyond the scope of the current study. We will be exploring this issue in future work by searching for abundance gradient using spatially resolved X-ray spectral data.

We initially explored values for E_0 and n searching for model remnants that attained radii between 12 pc and 14 pc in ages of from 19,000 yr to 25,000 yr. This requirement largely constrained the ratio of E_0/n to be $\sim(0.2 - 0.4) \times 10^{51}$ ergs cm^3. Next this range of model parameters was explored more finely in order to find SNRs that reproduced both the measured X-ray intensity and a centrally-peaked surface brightness profile. The model temperature and density profiles were projected as above using the best-fit ISM column density ($N_H = 1.0 \times 10^{22}$ atoms cm^{-2}) to obtain surface brightness profiles in terms of PSPC counts s^{-1} arcmin^{-2} for comparison to the data. Appropriate values of E_0 in the range $(0.1 - 2) \times 10^{51}$ ergs and n in the range $0.25 - 11$ cm^{-3} were considered. The best fit solutions to the W44 data were obtained for $E_0 \approx (0.5 - 0.7) \times 10^{51}$ ergs and $n \approx (2.0 - 3.3)$ cm^{-3}. Figure 4 shows the radial X-ray surface brightness profiles of several of these acceptable models.

The curves (labelled "a" and "b") show how the X-ray surface brightness profile varies with age. The top curve is the model with $E_0 = 0.6 \times 10^{51}$ ergs and $n = 2.5$ cm^{-3} at 19,400 yr and the bottom one is the same case at 25,200 yr. In these models there is a dense shell of radiatively cooled ISM at radii of 13.0 pc (a) or 14.1 pc (b) at the outer edge of the remnant. Interior to this the temperature rises slowly, increasing from about 10^6 K just inside the radiative shell to 10^7 K near the center. Over the same radial range the density shows a gradient of the opposite sign, decreasing from the edge of the remnant in toward the center. The centrally bright profile is a result of absorption by the large column density to W44 of the soft X-rays from near the remnant edge. The harder photons from the hotter gas in the interior are preferentially less absorbed and thus, although the matter density is less there, have a higher observed emissivity. The other curves in Figure 4 show the X-ray brightness profiles of models with other values for E_0 and n.

It has occasionally been suggested that shock models would provide a poor explanation of the centrally-peaked SNRs since such models are expected to show significant radial temperature gradients. We have examined the emission-measure-weighted projected

temperature of our model labeled "a" in Figure 4 and find that over the flat part of the profile the temperature varies from 0.58 keV at the center to 0.44 keV near the edge. This modest variation is fully consistent with the limits we set of 10%–20% variation in temperature from the PSPC data (§3.2).

It is remarkable that this very simple model, a function of only two parameters, reproduces both the observed intensity of the remnant and, at least to first approximation, the centrally peaked X-ray brightness profile. The derived parameters, in particular an explosion energy of $\sim 0.6 \times 10^{51}$ ergs, are physically quite plausible. And since the remnant's age is similar to the characteristic age of the pulsar, there is no need to invoke an unusual evolutionary scenario for the spin-down of the pulsar. Because of these considerations, we favor this, the radiative phase shock model, for the interpretation of the center-filled X-ray emission from W44.

However this model is not a completely successful description of the current data. The emission-measure-weighted average temperatures of the acceptable shock models are in the range 0.4 keV to 0.5 keV, somewhat less than our observed value of $kT = 0.88 \pm 0.12$ keV. On the other hand the model temperatures are more consistent with a preliminary analysis of *ASCA* data that shows a mean temperature of 0.5 ± 0.2 keV (Harrus et al. 1996) for the hot plasma in W44. Clearly more careful analysis of the *ASCA* data will be crucial to further our understanding of the nature of W44 and the other filled-center remnants.

5. Summary

In this article we have presented an analysis of X-ray data from the *Einstein* SSS, the *ROSAT* PSPC, and the *Ginga* LAC on the supernova remnant W44. These spectral data are well described by a single-temperature, single-timescale nonequilibrium ionization model with temperature 0.88 ± 0.014 keV and ionization timescale $(2.0^{+4.3}_{-0.7}) \times 10^{11}$ cm^{-3} s, observed through a large absorbing column density: $N_{\mathrm{H}} = (1.0^{+0.6}_{-0.2}) \times 10^{22}$ atoms cm^{-2}. All elemental abundances are close to the solar values, with iron possibly appearing to show significant depletion.

Morphologically W44 belongs to the class of SNRs that have clear shell-like structures in the radio but are centrally-peaked in the X-ray band with thermal spectra. We have examined in detail two proposed scenarios for the origin of this structure: (1) a model specifically developed for application to this class of remnants invoking a long evaporative timescale for the destruction of clouds engulfed by the SN blast wave (White & Long 1991) and (2) a model of remnant evolution in a homogeneous medium during the post-Sedov phase of development when radiative cooling at the shock front has become important. Because W44 is such a well-studied object there is a wealth of information available on

it. The distance is accurately known and, since there is an associated pulsar, we have an independent estimate of the age of the remnant. Our measurement of the mean temperature of the hot plasma in W44 from the X-ray observations, coupled with its age and size, is what provides the strongest constraints on the evolutionary state of the remnant.

Taking the size and temperature as the fundamental observables, we find that the WL model predicts an age of 5600–7500 yr, which is incompatible with the characteristic age ($\sim$20,000 yr) of the associated pulsar PSR 1853+0.1. This is considerably greater than any discrepancy that could be resolved though errors in the distance to W44 or the X-ray temperature measurements. It would require that the pulsar in W44 to have been born as a slow rotator ($P_0 \gtrsim 200$ ms) or to have undergone an unusual spin-down history. The WL model also predicts an unusually low explosion energy $\lesssim 0.2 \times 10^{51}$ ergs for the core-collapse SN that is believed to have formed W44 and PSR 1853+0.1. These two observationally-derived conclusions are the basis on which we reject this model as the explanation of the center-filled remnants in favor of the radiative shock phase model. However, we also wish to highlight the astrophysical implausiblity of a major assumption of the WL model, i.e., that the ISM clouds engulfed by a SNR should survive being crushed by the blast wave and linger within the interior to be gently evaporated away on timescales that are many times the age of the remnant. We do not reject the WL model because we consider a cloudy ISM unlikely, rather it is the *timescale* for the destruction of those clouds that is at issue.

Our alternative scenario for W44 has the remnant in the post-Sedov radiative phase of evolution. In this case we find that a centrally-peaked morphology and nearly uniform temperature profile can occur for models that are roughly 19,000 yr to 25,000 yr old for reasonable explosion energies ($\sim$0.6 $\times 10^{51}$ ergs) and ISM densities of 2.5–3.3 cm^{-3} (assumed uniform and homogeneous). These are not outrageously large values for the ambient density, rather they are very similar to the ambient densities estimated around the SNRs N132D and N49 in the Large Magellanic Cloud (Hughes 1987; Vancura *et al.* 1992). The reason for these largish densities is attributed to the presence of nearby molecular clouds for the LMC SNRs (Banas et al. 1996). A similar explanation is likely for W44, since it too appears to be associated with molecular emission (Wootten 1977).

Additional research on W44 should be directed toward obtaining spatially resolved measurements of temperature and elemental abundance. This will be a challenging measurement to make since both the radiative phase model and the current data support the presence of only a modest radial variation in temperature. We are pursuing this issue further with the available *ASCA* data. It is also interesting to note that a more accurate estimate of the remnant's age may become available in the future. Recently, Frail et al. (1996) have argued that the pulsar in W44 is moving toward the south with a speed of approximately 375 km s^{-1}. Since the likely location of the SN explosion which gave rise

to the pulsar is known (i.e., the centers of the radio, X-ray, and H I images of W44), measurement of the proper motion of PSR 1853+0.1 (estimated to be of order 25 mas yr^{-1}) would provide a distance-independent determination of the age of the pulsar and the SNR. As we have shown in this article, such a definitive measurement would yield a crucial constraint on models for the evolutionary state of W44 and should be pursued.

REFERENCES

Banas, K. R., Hughes, J. P., Bronfman, L., & Nyman, L.-Å. 1996, ApJ, submitted

Boyd, P. T., et al. 1995, ApJ, 448, 365

Christian, D. J., Swank, J. H., Szymkowiak, A. E., & White, N. E. 1992, Legacy, 1, 38

Cox, D. P. 1972, ApJ, 178, 159

Edge, D. O., Shakeshaft, J. R., McAdam, W. B., Baldwin, J. E., & Archer, S. 1959, MNRAS, 68, 37

Frail, D. A., Giacani, E. B., Goss, W. M., & Dubner, G. 1996, ApJ, 464, L165

Giacconi, R., et al. 1979, ApJ, 230, 540

Gronenschild, E. H. B. M., Mewe, R., Heise, J., Den Boggende, A. J. F., Schrijver, J., & Brinkman, A. C. 1978, A&A, 65, L9

Gross, W. M. 1968, ApJS , 15, 131

Gross, W. M., Caswell, J. L., & Robinson, B. J. 1971, A&A, 14, 481

Harrus, I., Hughes, J. P., & Helfand, D. J. 1996, ApJ, 464, L161

Hughes, J. P. 1987, ApJ, 314, 103

Hughes, J. P., & Helfand, D. J. 1985, ApJ, 291, 544

Hughes, J. P., Helfand, D. J., & Kahn, S. M. 1984, ApJ, 281, L25

Hughes, J. P., & Singh, K. P. 1994, ApJ, 422, 126

Hwang, U., Hughes, J. P., Canizares, C. R., & Markert, T. H. 1993, ApJ, 414, 219

Jones, L. R., Smith, A., & Angellini, L. 1993, MNRAS, 265, 631

Joyce, R. M., Becker, R. H., Birsa, F. B., Holt, S. S., & Noordzy, M. P. 1978, IEEE Transactions, 25, 453

Kaspi, V. M., Manchester, R. N., Siegman, B., Johnston, S., & Lyne, A. G., 1994, ApJ, 422, L83

Knapp, G. R., & Kerr, F. J. 1974, A&A, 33, 463

Koo, B.-C., & Heiles, C. 1995, ApJ, 442, 679

Kundu, M. R., & Velusamy, T. 1972, A&A, 20, 237

Long, K. S., Blair, W. P., Matsui, Y., & White, R. L. 1991, ApJ, 373, 567

Lyne, A. G., Pritchard, R. S., & Smith, F. G. 1993, MNRAS, 265, 1003

Lyne, A. G., Pritchard, R. S., Smith, F. G., & Camilo, F. 1996, Nature, 381, 497

Makino, F., and the Astro-C team 1987, Astrophys. Lett. and Communications, 25, 223

McKee, C. F. & Ostriker, J. P. 1977, ApJ, 218, 148

Mills, B. Y., Slee, O. B., & Hill, E. R. 1958, Aust. J. Phys., 11, 360

Mohanty, D. K. 1983, in IAU Symposium 101, Supernova Remnants and their X-ray Emission, ed. J. Danziger & P. Gorenstein (Dordrecht: Reidel), p. 503

Morrison, R., & McCammon, D. 1983, ApJ, 270, 119

Pfeffermann, E., et al. 1986, Proc SPIE, 733, 519

Radhakrishnan, V., Goss, W. M., Murray, J. D., & Brooks, J. W. 1972, ApJS, 24, 49

Raymond, J. C., Cox, D. P., & Smith, B. W. 1976, ApJ, 204, 290

Raymond, J. C., & Smith, B. W. 1977, ApJS, 35, 419 (RS)

Rho, J. H., Petre, R., Schlegel, E. M., & Hester, J. J. 1994, ApJ, 430, 757

Scheuer, P. A. G. 1963, Observatory, 83, 56

Sedov, L. I. 1959, Similarity and Dimensional Methods in Mechanics (New York: Academic)

Seward, F. D., Schmidt, B., & Slane, P. O. 1995, ApJ, 453, 284

Smith, A., Jones, L. R., Watson, M. G., Willingale, R., Wood, N., & Seward, F. D. 1985, MNRAS, 217, 99

Snowden, S. L., McCammon, D., Burrows, D. N., & Mendenhall, J. A. 1994, ApJ, 424, 714

Taylor, J. H., Manchester, R. N., & Lyne, A. G. 1993, ApJS, 88, 529

Taylor, J. H., & Cordes, J. M. 1993, ApJ, 411, 674

Thielemann, F.-K., Nomoto, K., & Hashimoto, X. 1996, ApJ, 460, 408

Trümper, J. 1983, Adv. Space Res., 2, 241

Turner, M. J. L., et al. 1989, PASJ, 41, 345

Vancura, O., Blair, W. P., Long, K. S., & Raymond, J. C. 1992, ApJ, 394, 158

Vancura, O., Raymond, J. C., Dwek, E., Blair, W. P., Long, K. S., & Foster, S. 1994, ApJ, 431, 188

Westerhout, G. 1958, Bull. Astron. Inst. Netherlands, 14, 215

Wheeler, J. C. 1981, Rep. Progr. Phys., 44, 85

White, R. L., & Long, K. S. 1991, ApJ, 373, 543 (WL)

Wolszczan, A., Cordes, J. M., & Dewey, R. J. 1991, ApJL, 372, 99

Wolszczan, A. 1995, private communication

Wootten, H. A. 1977, ApJ, 216, 440

Table 1. Elemental Abundances of W44

Species	Best fit relative to $\odot$	Random Error	Error due to variation with:		
			N_{H}	$n_e t$	kT
Ne	0.76	+0.35 / −0.35	+0.18 / −0.78	+0.20 / −0.15	+0.40 / −0.10
Mg	0.90	+0.33 / −0.25	+0.80 / −0.10	+0.50 / −0.10	+0.60 / −0.10
Si	0.70	+0.21 / −0.16	+0.25 / −0.05	+0.15 / −0.05	+0.20 / −0.10
S	0.64	+0.28 / −0.20	+0.15 / −0.05	+0.15 / −0.05	+0.15 / −0.05
Ar	0.24	+0.40 / −0.15	+0.15 / −0.05	+0.10 / −0.05	+0.15 / −0.05
Fe	0.07	+0.08 / −0.07	+1.10 / −0.07	+0.35 / −0.07	+0.65 / −0.07

Fig. 1.— The top panel shows the X-ray spectra of W44 from the *ROSAT* PSPC, *Einstein* SSS, and *Ginga* LAC with the best-fit single-temperature, single-timescale nonequilibrium ionization model. The residual spectrum (observed data minus best-fit model) is shown in the bottom panel.

Fig. 2.— The effect of variation in column density (N_H), temperature (kT), and ionization timescale ($n_e t$) on the best-fit emission measures of the various species considered from fits to the W44 X-ray spectra using the nonequilibrium ionization model. The top three panels show the change in χ^2 with the independent variation of each spectral parameter. The 90% confidence interval (for three interesting parameters) is shown in each panel as a dashed line ($\chi^2_{min} + 6.25$). The variations of elemental abundance (relative to the appropriate solar value) are shown in the bottom panels. The error bars are plotted at the best-fit values and represent the random error at 90% confidence.

Fig. 3.— Radial X-ray surface brightness profile of W44 from the *ROSAT* PSPC (shown as the 7 data points with statistical error bars) compared to the White and Long (1991) similarity solution for the evolution of SNRs in a cloudy interstellar medium. The solid curves show acceptable fits while the dashed curves indicate the extremes of the allowed solutions. These models all predict a young age (5600–7500 yr) and low explosion energy $(0.11–0.16) \times 10^{51}$ ergs for W44.

Fig. 4.— Radial X-ray surface brightness profile of W44 from the *ROSAT* PSPC compared to radiative-phase shock models. The curves are labeled with the explosion energy (in units of 10^{51} ergs) and ambient ISM density (cm^{-3}) of the model as (E_0, n). The two curves delineating the dotted region labeled "a" and "b" show how the profile varies with remnant age from 19,000 yr (a) to 25,000 yr (b). All these models are consistent with the spin-down age of the associated pulsar PSR 1853+01, $P/2\dot{P} \sim 20000$ yr.